

Propagation of Ripples in Monte Carlo Models of Sputter Induced Surface Morphology

Oluwole E. Yewande,* Alexander K. Hartmann, and Reiner Kree

Institute for Theoretical Physics, University of Göttingen, Tammannstr. 1, 37077 Göttingen, Germany

(Dated: December 2, 2024)

Periodic ripples generated from the off-normal incidence ion beam bombardment of solid surfaces have been observed to propagate with a dispersion in the velocity. We investigate this ripple behaviour by means of a Monte Carlo model of the erosion process, in conjunction with one of two different surface diffusion mechanisms; one without and the other including a term that accounts for the Schwoebel effect. We find that the scaling of the ripple velocity and wavelength depends on the sputtering timescale, qualitatively consistent with experiments. Furthermore, we observe a strong temperature dependence of the ripple velocity, calling for experiments at different temperatures. Also, we observe that the ripple velocity vanishes ahead of the periodic ripple pattern.

PACS numbers: 05.10.-a,68.35.-p,79.20.-m

I. INTRODUCTION

There has been much scientific activity for quite some time now, on the features of surface morphology resulting from the bombardment of a solid surface by a collimated beam of intermediate energy ions, at normal and oblique incidence to the solid surface [1, 2]. The phenomenon is an essential constituent of several surface analysis, processing and fabrication techniques, such as ion beam aided deposition, surface catalysis, sputter cleaning, etching and deposition.

Normal incidence ion bombardment of non-metallic substrates often results in an interlocking grid of hillocks and depressions, which have been demonstrated to be an attractive alternative to the spontaneous growth of self-organized quantum dots on semiconductor surfaces in the Stranski-Krastanov growth mode [3]. Off-normal incidence ion bombardment of such non-metallic substrates, however, gives rise to the formation of quasiperiodic ripples [4, 5, 6, 7, 8, 9, 10, 11] with orientation that depends on the angle of incidence of the ion beam. For incidence angles less than a critical angle, θ_c [12], the wavevector of the ripples is parallel to the projection of the ion beam direction on the surface plane while for incidence angles greater than θ_c , the wavevector of these ripples is oriented perpendicular to the projection of the ion beam direction on the surface plane. On the other hand, ripples are observed on metallic substrates at normal incidence ion bombardment, and these ripples are rotated by changing the substrate temperature [13, 14, 15]; a probable consequence of the symmetry-breaking anisotropy in surface diffusion. The wavelengths of the observed ripples, in all cases, is of the order of tenths of micrometers.

However, a number of experimental studies [16, 17, 18, 19] have demonstrated that under certain ion bombardment conditions, ripples are not formed; the surface undergoes kinetic roughening with interesting scal-

ing properties. All these observations point to the possibility of several phases in the surface topography evolution, with phase boundaries defined by the bombardment conditions, and with little or no dependence on the material composition, surface chemistry, defects or chemical reactions on the surface. These features are understood, from insightful theoretical descriptions [2, 20, 21], as being governed by the interplay and competition between the dynamics of surface roughening on the one hand and material transport during surface migration on the other. For sufficiently low ion energies, the sputtering phenomenon is the dominating mechanism [2].

Recently surface ripples generated during Gallium ion beam erosion of Silicon were observed to propagate with a ripple velocity that scales with the ripple wavelength as $v \sim \lambda^k$, where $k \simeq 0$ initially, and $k = -1.5$ after a crossover wavelength $\lambda_c \simeq 100\text{nm}$ [22]. This velocity dispersion has been ascribed to an indication of a continuous transition to a rising non-linear contribution in surface erosion [2, 22]. Motivated by this experimental result, we study ripple propagation by means of a recently introduced, discrete (2+1) dimensional Monte Carlo model [23] of the sputtering process, and two different solid on solid models of surface diffusion; with or without the Schwoebel effect. We focus on intermediate times, where the transition from linear to non-linear regimes occur. Our results corroborate the experimental observation, but in addition, we find that the ripples first come to rest before they are completely wiped out by the increasing non-linear contributions.

The rest of the paper is organized as follows. First, we state our simulation model, i.e. how the sputtering process and the different diffusion mechanisms are implemented. Then we explain, how we study the movement of the ripples. In the main section, we show our simulation results. We finish with our conclusions and an outlook.

*Electronic address: yewande@theorie.physik.uni-goettingen.de

II. EROSION AND SURFACE MIGRATION

According to Sigmund's sputtering theory [24], the rate at which material is removed from a solid surface, through the impact of energetic particles, is proportional to the power deposited there by the random slowing down of particles. The average energy $E(\mathbf{r}')$ deposited at surface point $\mathbf{r}' = (x', y', -z')$ is given by the Gaussian distribution

$$E(\mathbf{r}') = \frac{\epsilon}{(2\pi)^{3/2}\sigma\mu^2} \exp\left(-\frac{(z'+d)^2}{2\sigma^2} - \frac{x'^2+y'^2}{2\mu^2}\right) \quad (1)$$

where we have used the local Cartesian coordinate system of the ion with origin at the point of penetration and with the z axis coinciding with the ion beam direction; $(z'+d)$ is the distance of the surface point, from final stopping point of ion, measured along the ion trajectory, $\sqrt{x'^2+y'^2}$ is the distance perpendicular to it; σ and μ are the widths of the distribution parallel and perpendicular to the ion trajectory respectively; ϵ is the total energy deposited, d is the average depth of energy deposition.

A. The Sputtering Process

Following [23], we simulate the sputtering process on a surface of size L^2 with periodic boundary conditions, by starting an ion at a random position in a plane parallel to the plane of the initially flat surface, and projecting it along a straight trajectory inclined at angle θ to the normal to the average surface configuration; at an azimuthal angle ϕ . The ion penetrates the solid through a depth d and releases its energy, such that an atom at a position $\mathbf{r} = (x, y, h)$ is eroded (see Fig. 1 of [23]) with probability proportional to $E(\mathbf{r})$. It should be noted that, consistent with the assumptions of the theoretical models [2, 20, 21], this sputtering model assumes no evaporation, no redeposition of eroded material, no preferential sputtering of surface material at point of penetration, and surface is defined by a single valued, discrete time dependent height function $h(x, y, t)$ (solid-on-solid model, SOS). The time t is measured in terms of the ion fluence; i.e., number of incident ions per two-dimensional lattice site (x, y) . We used incidence angle $\theta = 50^\circ$, azimuthal angle $\phi = 22.0^\circ$, $d = 6.0$, $\sigma = 3.0$, $\mu = 1.5$; which according to the linear theory of Bradley and Harper, should give $\theta_c = 68^\circ$ [12]. We have chosen ϵ to be $(2\pi)^{3/2}\sigma\mu^2$, which leads to high sputtering yields $Y \simeq 7.0$ compared to experiments like [11], where $Y = 0.3, \dots, 0.5$, i.e. increasing the efficiency of the simulation. According to the Bradley Harper theory, the ripple wavelength λ scales like $\lambda \sim Y^{-1/2}$ so that we expect patterns with correspondingly smaller length scales in our simulations. This we have to remember when quantitatively interpreting the result. Anyway, the general phenomena observed in the simulation are not affected by this choice.

B. The Hamiltonian and Arrhenius Models of Surface Diffusion

Surface migration is modelled as a thermally activated nearest neighbor hopping process, as in [25, 26]. One diffusion step refers to a complete sweep of the lattice. Two different solid-on-solid models of surface diffusion in molecular beam epitaxy are used; the second one of them sensitive to the repulsion of a diffusing particle from a down step, and preferential diffusion in the uphill direction: the so-called Schwoebel effect.

In the first model [25], a site i and one neighbour site j are randomly selected. The trial move is an atom hopping from i to j , i.e. $h_i = h_i - 1$ and $h_j = h_j + 1$. We calculate the surface energy before and after the hop, through the energy of an unrestricted SOS model

$$E = \frac{J}{2} \sum_{\langle i,j \rangle} |h_i - h_j|^2 \quad (2)$$

J is a coupling constant through which the nearest neighbor sites interact. h_i is the height variable at site i , and the summation is over the nearest neighbors on the 2-dimensional substrate.

The hop is allowed with the hopping rate

$$p_{i \rightarrow f} = 1 / \left[1 + \exp\left(\frac{\Delta E_{i \rightarrow f}}{k_B T}\right) \right] \quad (3)$$

where $\Delta E_{i \rightarrow f}$ is the energy difference between the initial and final states of the move. T is the substrate temperature, and k_B is the Boltzmann's constant. Although no exact mapping is possible we can estimate that a temperature $k_B T / J \simeq 0.2$ in this model corresponds roughly to room temperature. The estimate is based on a comparison of this pure diffusion process with the second model of diffusion introduced below. Note that room temperature is below the roughening transition of this model [25]. This model does not prevent atoms from moving down over steps edges, hence no Schwoebel effect is present.

In the second model [26], again a site i and a nearest neighbor site j are chosen at random but now a hopping move is performed with a probability proportional to the hopping rate of an Arrhenius form

$$k(E, T) = k_0 \exp\left(-\frac{E}{k_B T}\right) \quad (4)$$

$E = E_{SB} + nnE_{NN} + E_S$ is an energy barrier to hopping, consisting of a Schwoebel barrier term E_{SB} , a substrate term $E_S = 0.75\text{eV}$ and a nearest neighbor bonding of magnitude $nnE_{NN} = nn0.18\text{eV}$; where nn is the number of in-plane nearest neighbors of the diffusing atom. E_{SB} is equal to some constant (0.15eV in this case), if the numbers of next-nearest neighbors in the plane beneath the hopping atom before (nnn_b) and after (nnn_a) the hop, obey $4 = nnn_b > nnn_a$; and zero otherwise. Our temperature is measured in units of $\text{eV}k_B^{-1}$ in this model, where $T \simeq 0.02\text{eV}k_B^{-1}$ corresponds to room temperature.

$k_0 = 2k_B T/h$ is the vibrational frequency of a surface adatom, i.e. a hopping attempt rate, h being Planck's constant. The hopping attempt rate is very high, with a corresponding low hopping probability resulting from Eq. 4, slowing down the simulation. Thus we incorporate the factor $\exp(-E_S/k_B T)$ into the rescaled attempt rate such that the hopping rate reads

$$k(E, T) = k_1 \exp\left(-\frac{\Delta E}{k_B T}\right) \quad (5)$$

where $k_1 = k_0 \exp\left(-\frac{E_S}{k_B T}\right)$ is a much lower hopping attempt rate, $\Delta E = nnE_{NN} + E_{SB}$. Note that for atoms on top of planes, which are far from down edges, $\Delta E = 0$, i.e. each hop is accepted, independently of the temperature.

III. RIPPLE KINEMATICS

In experiments, we typically have $N = 1 \times 10^{15} \text{ atoms/cm}^2$ on the surface. Since the typical experimental ion current density is of the order $F = 7.5 \times 10^{14} \text{ ions/cm}^2 \text{s}$ [22], this implies a flux of $\Phi = F/N \simeq 0.75 \text{ ion/atom s}$. From the values given above, we get hopping attempt rates k_1 of around 200 1/s for room temperature, hence 200 sweeps of the diffusion mechanism correspond to 0.75 ions per surface atom. Thus, we initiate a diffusion step every $\Phi L^2/k_1 = 0.0037 L^2$ erosion steps; L is the system size.

Initially, for times less than about 1.4 ions/lattice site, the surface is rough [23] and then the formation of ripples starts. In this paper we focus on the motion and time development of these ripples. In Fig. 1 the time development of a sample surface topology is shown for the first diffusion model. Initially ripples are formed. They propagate slowly and, due to the increasing influence of non-linear effects (note the scales at the right), disappear at longer times. The long-time behavior, where the ripples have disappeared, has already been studied in Ref. 23.

In order to monitor the ripple propagation on the computer, we assign the crest points of the ripples to clusters, and then monitor the motion of these clusters. A cluster of crest points is defined as the set of surface points with height $h(x, y, t) \geq h_c$ and nearest neighbor distance $l \leq l_c$, where h_c and l_c are cut-off surface height and distance between neighboring cluster points respectively. We have chosen our cut-off height to be a function of the average height of the configuration $\langle h \rangle$, and the height difference h_d between the maxima and minima of the surface; i.e. $h_c = \langle h \rangle + ph_d$, where p is some fixed percentage. In this way clusters with about the same proportionate sizes can be followed from the beginning of ripple formation until complete disappearance of the ripples. Furthermore, we have used $l_c = 2$. Different, unconnected ripples should, in general, generate different clusters. We

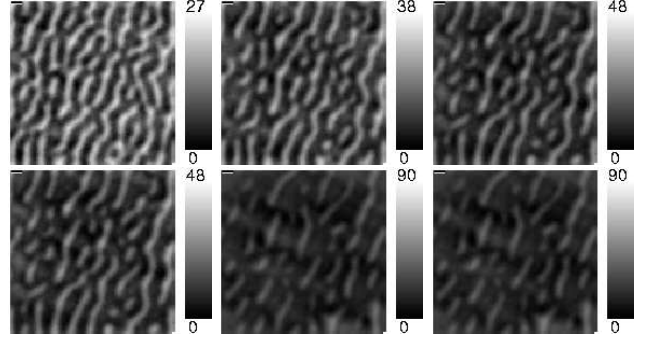


FIG. 1: Surface profiles at a substrate temperature of $0.2 J/k_B$ and at different times. Starting from top-bottom, left-right, $t=3, 5, 7, 10, 15$, and 20 ions/atom. Ion beam direction is perpendicular to ripple orientation, at an angle of $\phi = 22^\circ$ from upper horizontal boundary of profile. The scales show the surface height measured from the lowest height.

also require that the number N of elements in a cluster be large enough to allow for statistical analysis, here we have chosen $N \geq 10$ elements.

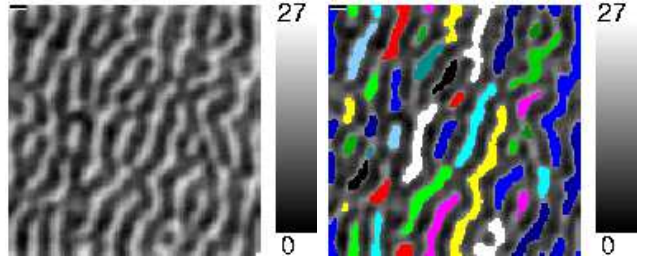


FIG. 2: Surface profile for time 3 ions/atom (no Schwoebel barrier, $T = 0.2 J/k_B$, $L = 128$). The second profile contains the clusters formed from the first profile, as described in the text.

The propagation of the ripples is studied by calculating the time rate of change of the position of the centre of mass of a cluster

$$\dot{\mathbf{x}}_{CM} = \frac{\sum_i m_i \dot{\mathbf{x}}_i}{\sum_i m_i} \quad (6)$$

where the summation is over all the elements of the cluster. We have assumed a homogeneous system composed of unit mass particles, such that the center of mass of a cluster is $\mathbf{x}_{CM} = N^{-1} \sum_i \mathbf{x}_i$. The ripple wavelength is given by $\lambda = 2\pi/\eta$, η being the average expectation value of the Gaussian fitted to the peak of the structure factor $S(\mathbf{k}) = |h(\mathbf{k})|^2$, where $h(\mathbf{k})$ is the fourier transform of the height topography $h(\mathbf{r}, t)$, given by

$$h(\mathbf{k}) = \frac{1}{L^{d'/2}} \sum_{\mathbf{r}} [h(\mathbf{r}, t) - \langle h \rangle] e^{i\mathbf{k}\mathbf{r}} \quad (7)$$

d' is the substrate dimension, i.e. here $d' = 2$. Fig. 2 shows two profiles of the surface for system size 128x128 at time $t = 3$ ions/atom; in the second profile, we print

the clusters on top of their corresponding ripples. As seen in the figure of the clusters, application of periodic boundary conditions necessitates the need to first unfold toroidal clusters before calculating the position of their center of mass. As time increases, local surface slopes ∇h increase, and since the non-linear effects depend on the square of ∇h they will dominate by scaling down surface relaxation mechanisms [1]. These non-linear effects are responsible for the disappearance of ripples (Fig. 1) at long times, and for the transition of the surface topography from a periodic ripple pattern to a rough topography with self-affine scaling [2, 16]. We thus expect fluctuations in the position of the centre of mass due to disappearing ripples; the fluctuations are averaged out by using systems of size 512x512 with a large number of clusters such that the ripple velocity at any time is an average of the velocities of all the ripples at this time.

IV. RESULTS AND DISCUSSION

The results are obtained, as already mentioned, for square lattices of size 512x512, with periodic boundary conditions, and as an average over fifty different realizations.

The simulations for the case including the Schwoebel barriers for room temperature $k_B T = 0.02\text{eV}$, yield structures shown in Fig. 3, for intermediate as well after long sputtering times. We cannot observe clean ripples. The reason is that this kind of diffusion mechanism is too slow at room temperature to effectively counteract the strong roughening due to our model of sputtering, which possesses a particularly high sputtering yield. Hops are almost always prevented if an atom has in-plane neighbours, so the mechanism is not very effective on a rough surface. Since the surface relaxation is essential for the formation of ripples [20], it needs higher than room temperatures to produce clean ripples in our model. This is different from the mechanism resulting from Eq. (3), where moves smoothing the surface, i.e. decreasing the energy, are not hampered by in-plane neighbors. Hence, for the further analysis of ripple movement, we consider higher temperatures for the model including Schwoebel barriers, such that the surface diffusion may act as an effective smoothing mechanism (see Fig. 4). At such higher temperatures we observe some universal features both for the diffusion with and without Schwoebel barriers.

Figures 5 and 6 are plots of the ripple wavelength (line with circle symbols) as a function of time measured in units of the number of ions per atom. The results in Figs. 5 and 6 are obtained by using the first and second models of surface diffusion, i.e without and with the Schwoebel effect, respectively. Considering the lifetime of the ripples from first appearance to annihilation, the wavelength increases exponentially with time as $\lambda \sim \exp(\rho t)$, $\rho = 0.029$ (Fig. 5), in the first model, while it increases with time according to the inverse law $\lambda(t) \approx g(t) = 1/(c_1 - c_2 t)$

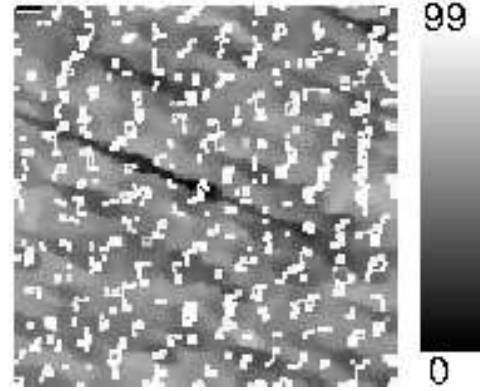


FIG. 3: Sample surface topology for a small system ($L=128$), when including Schwoebel barriers at room temperature, after $t = 100$ ions/atom. No clear ripples can be observed. Similar results were observed for almost all time, except the very early ones.

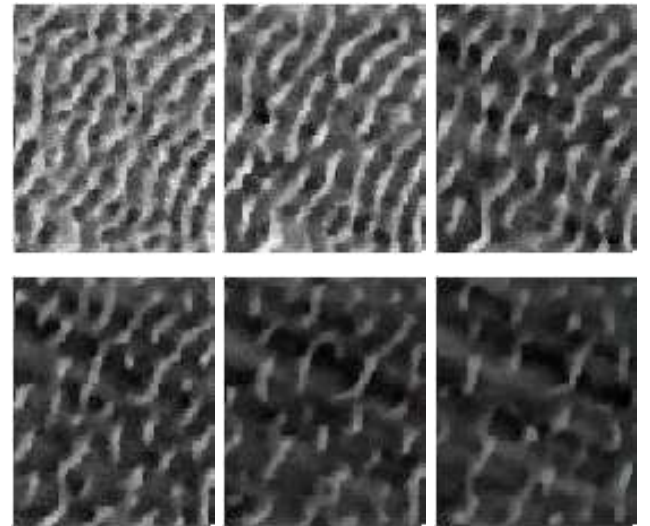


FIG. 4: Surface profiles at a substrate temperature of $0.2\text{eV}/k_B$ with the second diffusion model. Starting from top-bottom, left-right, $t=1.5, 3.0, 4.5, 6.0, 9.0$, and 12.0 ions/atom.

with $c_1 = 0.083$ and $c_2 = 0.0036$ (Fig. 6) in the second model. Note that these fits are purely heuristic. We are not aware of any theory of the time dependence of ripple wavelength and velocity, only a calculation of the dispersion relation $v(\lambda)$ has been performed within linear theory [2]. However, experiments by Habenicht et al. [22] and Frost et al. [27] obtained power law behavior in the wavelength-time relationship. We can get similar power laws if we restrict ourselves to specific regions in time, but the scaling will be strongly dependent on the timescale. For instance, on performing a power law fit $\lambda \sim t^\gamma$ within the region $t = 4 - 12$ ions/atom (where the ripple velocity exhibits a power-law behavior as well), we found $\gamma = 0.19$ (Fig. 5) and $\gamma = 0.43$ (Fig. 6), without

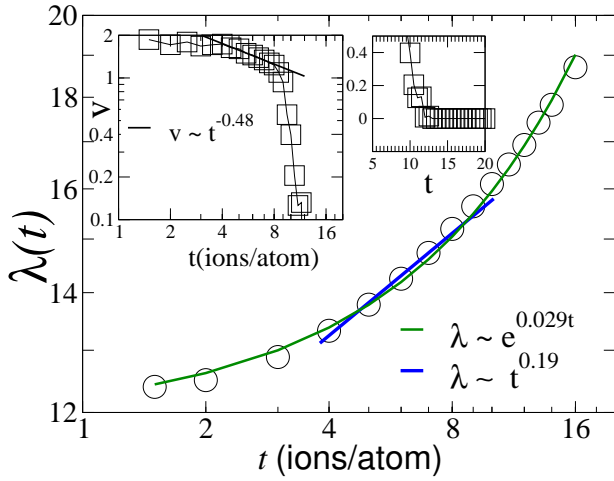


FIG. 5: Ripple wavelength, λ , measured in lattice units, as a function of time, t . The inset shows the time dependence of the ripple propagation velocity, v (measured in lattice units per ion per atom); the smaller inset shows that the ripples finally come to rest. Both results are without Schwoebel effect, at a substrate temp of $0.2 Jk_B^{-1}$

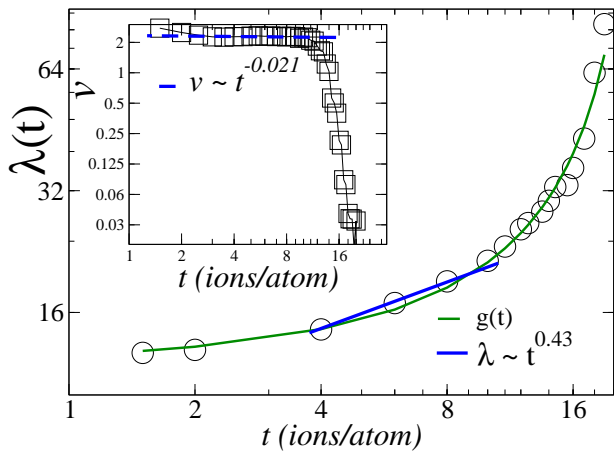


FIG. 6: Same plot as in Fig. 5 but with Schwoebel energy barriers, for a substrate temperature of $0.2 Jk_B^{-1}$. In both figures, the line with circle symbols represent the wavelength while the line with square symbols represent the velocity. The function $g(t)$ is given in the text.

and with Schwoebel effect respectively. But note that the result $\lambda \sim t^{0.19}$ (Fig. 5) in the first model, is closer to the experimental result $\lambda \sim t^{0.26}$ of Frost et al. [27]; while that of the second model, $\lambda \sim t^{0.43}$ (Fig. 3) is closer to the experimental result $\lambda \sim t^{0.5}$ of Habenicht et al. [22].

The insets of Figs. 5 and 6 are plots of the ripple velocity (line with square symbols) as a function of time. Irrespective of whether Schwoebel effect is accounted for, or not, the velocity is at first almost independent of time, then it disperses after a transition time t_r . But specif-

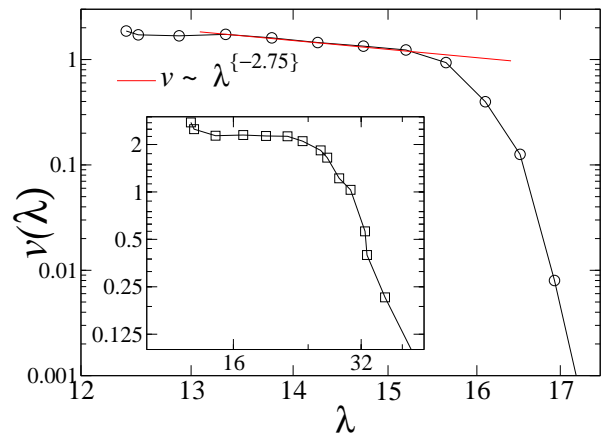


FIG. 7: Ripple velocity as a function of ripple wavelength, without and, in the inset, with Schwoebel barriers.

ically in the region $t = 4 - 12$ ions/atom, for the diffusion model Eq. (3), the velocity scales as $t^{-0.48}$, while the experimental result is an exponent -0.75 [22]. Figure 7 shows the dependence of the ripple velocity on the wavelength, their order of magnitude relationship is about the same as in the experiment. Our scaling exponent of -2.75 , obtained in the low-fluence region, where a power-law scaling can be observed here, is in better agreement with the theoretical result, based on linear approximation of continuum models, where $v \simeq \lambda^{-2}$ for long wavelength modes. We see in Fig. 8 that the trend in velocity variation is the same at different temperatures but the magnitude increases with temperature, as one would expect from the temperature dependence of the surface diffusion. These results are in qualitative agreement with the experimental results and theoretical predictions [2, 20, 21, 22, 27]. But we can observe a power-law scaling only for small time windows, if at all. This indicates that the presence of power-law scaling of ripple wavelength and velocity, and the corresponding exponents, depend on the time scale of observation, as well as on the substrate temperature.

It seems that the increase in magnitude of the velocity, when measured at same time ($t < t_r$) but different temperatures, does not continue indefinitely in our model. In the upper graph of Fig. 8 there is very little difference in the magnitudes of the velocity at temperatures 2.0 and $5.0 Jk_B^{-1}$; even though the temperature difference is very high. This saturation behaviour is also displayed in the ripple wavelength at the same higher temperatures, as seen in the lower graph of Fig. 8. In principle, one can still fit an exponential law to the data, except that the decay constant ρ in the exponential becomes very small (It has the respective values of $0.029, 0.018, 0.0031$, and 0.003 from the lowest to the highest temperature.) So for

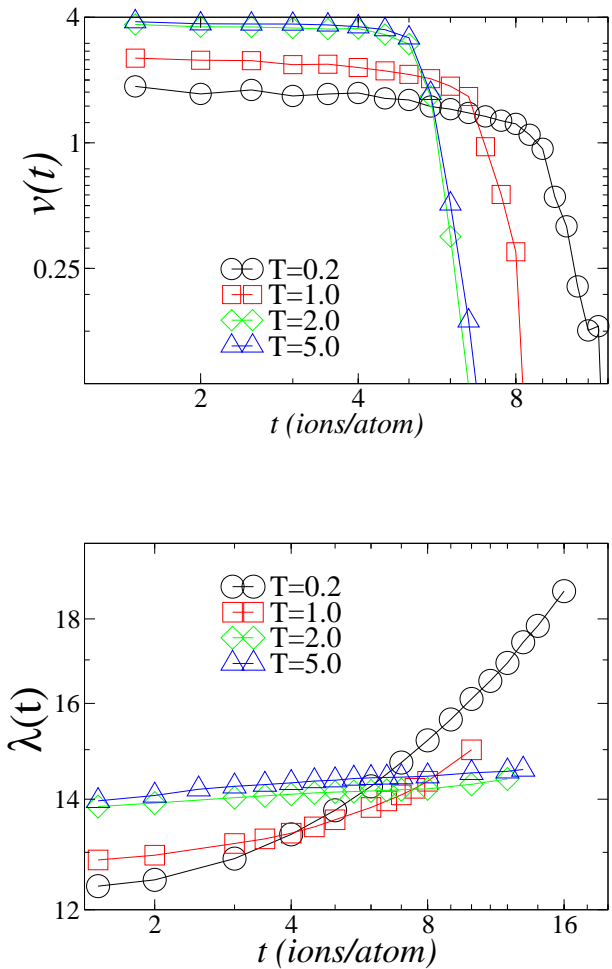


FIG. 8: Temperature dependence of the ripple velocity (upper graph), and ripple wavelength (lower graph); without the Schwoebel effect. Temperature is in units of Jk_B^{-1} for the upper plot and in units of eV/k_B for the lower one.

high temperatures we could equally well fit a power-law. Hence, there may be some “critical substrate temperature”, above which the wavelength remains nearly constant in time; and the velocity, after some time t_r , drops instantaneously to zero. Nevertheless, the temperature where such a “transition” will take place, is probably unphysically high (see below), so that the material would start to evaporate before reaching this point. So far, we are only aware of experiments at room temperature [22]. Hence, it would be very interesting to see, whether some temperature dependence of the dynamical features, including the disappearance of the coarsening, can be seen in experiments at higher temperatures.

Our results for the second diffusion model also indicate that in $\lambda(t) \approx 1/(c_1 - c_2 t)$, c_2 approaches zero with increasing temperature. Here, where we can measure the

temperature in real units, it is clear that the “transition” to almost non-coarsening ripples, takes place at unrealistically high temperatures $2-5eV/k_B$, where the material starts to evaporate. Moreover, we notice in Fig. 8 that the transition time from linear regime to onset of nonlinearities decreases with increasing temperature.

To summarize, immediately after ripple formation, the ripples move with constant velocity for some time, after which they begin to decelerate (insets of Figs. 5, 6) At the same time the ripple structure is gradually washed out. The ripple wavelength is always increasing in time (Figs. 5, 6). After some time, depending on the diffusion model, the ripples stop moving but keep disappearing gradually. In the final stage the ripples are completely wiped out.

V. CONCLUSION AND OUTLOOK

We have studied the propagation of ripples by means of a discrete $(2+1)$ -dimensional model of the sputtering process, combined with one of two different solid-on-solid models of surface diffusion: with and without Ehrlich-Schwoebel barriers. We have obtained the formation and propagation of the ripples with both diffusion mechanisms used in turn. Furthermore, we have obtained the same trend in the behavior of ripple velocity and wavelength as observed experimentally and predicted theoretically, but, in addition to the experimental results, we find that the ripples first stop moving before vanishing completely. We find that the behavior of the ripple velocity is characterized by two regions, separated at the transition time. In the first region it is constant and in the second region it decreases rapidly to zero. Between the two regions a power-law dependence can be observed for some time interval. On the other hand the wavelength increases exponentially with time in the model without Schwoebel barriers and obeys an inverse law if Schwoebel barriers are present. In addition, we find strong dependencies on the substrate temperature; as the temperature increases the magnitude of the velocity also increases. The transition time between constant and decreasing velocity is also found to decrease with increasing temperature. Our results indicate an approach towards a saturation behaviour of velocity or wavelength with increasing substrate temperature, where the wavelength is expected to become time independent. However, this may happen at an unphysically high temperature. Anyway, an experimental study of the temperature dependence of the dynamical features of ripple formation and effacement seems very promising.

One open problem of our model is that it uses the Sigmund formula for modeling the sputtering process. In a recent simulation [28] using a binary collision approximation, we observed that close to the penetration point of the ion, much less atoms were sputtered than predicted by the Sigmund formula (1), in fact the distribution shows a minimum there. When incorporating this

effect in the Bradley-Harper linear theory [20] of sputtering, one e.g. observes [28] that the sputter yield, i.e. the number of removed atoms per ion, exhibits a minimum for grazing incidence, like in experiments, in contrast to the original linear theory [20]. Hence, it may be promising to apply a different formula describing the sputtering, which takes into account this effect. Maybe the differences to experiments observed here, can then be removed.

Furthermore, the role of the interplay between the surface diffusion process and the sputtering process is still not fully understood. So far, we know that including a pure $T = 0$ relaxation in our sputtering model does not [23] lead to a disappearance of ripples for long times. Next, we know from this study, that one approach including calibrated Schwoebel barriers does not yield ripples at room temperature for sputtering yield $Y \approx 7$. There are

several different models [25, 26, 29, 30, 31, 32, 33, 34] for surface diffusion, which could be combined in a construction kit manner. Here, an extensive study over different combinations of parameters is necessary.

Finally, it would be of interest to include crystal anisotropy into the surface diffusion; This may give results in agreement with experimental studies of metallic substrates, which may be useful in understanding the anomalies of such surfaces.

Acknowledgements: The authors would like to thank K. Lieb and R. Cuerno for helpful discussions and suggestions. OEH thanks H. Löwe for interesting discussions. This work was funded by the DFG (*Deutsche Forschungsgemeinschaft*) within the SFB (Sonderforschungsbereich) 602 and by the *VolkswagenStiftung* (Germany) within the program “Nachwuchsgruppen an Universitäten”.

[1] A. -L. Barabási and H. E. Stanley, *Fractal Concepts in Surface Growth* (Cambridge University Press, Cambridge, 1995).

[2] M. Makeev, R. Cuerno and A. -L. Barabási, Nuc. Instr. and Meth. in Phys. Res. B **197**, 185 (2002).

[3] S. Facsko, T. Dekorsy, C. Koerdt, C. Trappe, H. Kurz, A. Vogt, and H. L. Hartnagel, Science **285**, 1551 (1999).

[4] T. M. Mayer, E. Chason, and A. J. Howard, J. Appl. Phys. **76**, 1633 (1994).

[5] E. Chason, T. M. Mayer, B. K. Kellerman, D. T. McIlroy, and A. J. Howard, Phys. Rev. Lett. **72**, 3040 (1994).

[6] C. M. Demanet, J. B. Malherbe, N. G. Vanderberg, and V. Sankar, Surf. Interface Anal. **23**, 433 (1995).

[7] S. W. MacLaren, J. E. Baker, N. L. Finnegan, and C. M. Loxton, J. Vac. Sci. Technol. A **10**, 468, (1992).

[8] J. B. Malherbe, CRC Crit. Rev. Solid State Mater. Sci. **19**, 55 (1994), and references therein.

[9] G. Carter, and V. Vishnyakov, Phys. Rev. B **54**, 17647 (1996).

[10] J. Erlebacher, M. J. Aziz, E. Chason, M. B. Sinclair, and J. A. Floro, Phys. Rev. Lett **82**, 2330 (1999) and references therein.

[11] S. Habenicht, W. Bolse, K. P. Lieb, K. Reimann, and U. Geyer, Phys. Rev. B **60**, R2200 (1999).

[12] According to the linear theory of Bradley and Harper, θ_c occurs at the point of intersection of the two functions $\Gamma_1(\theta) = \frac{\alpha}{\gamma} \{s - \frac{c}{2}[1 + \eta] - \frac{sc(\beta-\alpha)}{2\gamma}[3 + \eta]\}$ and $\Gamma_2(\theta) = \frac{\alpha c}{2\beta} \{1 + \frac{s(\beta-\alpha)}{\gamma}\}$; where $s = \sin^2(\theta)$, $c = \cos^2(\theta)$, $\alpha = (\frac{d}{\sigma})^2$, $\beta = (\frac{d}{\mu})^2$, $\gamma = \alpha s + \beta c$, $\eta = \frac{\alpha^2 s}{\gamma}$. d , σ and μ are as described in this paper. Depending on the choice of σ and μ there may be two critical angles [20].

[13] S. Rusponi, C. Boragno, and U. Valbusa, Phys. Rev. Lett. **78**, 2795 (1997).

[14] S. Rusponi, G. Costantini, C. Boragno, and U. Valbusa, Phys. Rev. Lett. **81**, 2735 (1998).

[15] S. Rusponi, G. Costantini, C. Boragno, and U. Valbusa, Phys. Rev. Lett. **81**, 4184 (1998).

[16] E. A. Eklund, R. Bruinsma, J. Rudnick, and R. S. Williams, Phys. Rev. Lett. **67**, 1759 (1991).

[17] E. A. Eklund, E. J. Snyder, and R. S. Williams, Surf. Sci. **285**, 157 (1993).

[18] J. Krim, I. Heyvaert, C. Van Haesendonck, and Y. Bruynseraede, Phys. Rev. Lett. **70**, 57 (1993).

[19] H. -N. Yang, G. -C. Wang, and T. -M. Lu, Phys. Rev. B **50**, 7635 (1994).

[20] R. M. Bradley and J. M. E. Harper, J. Vac. Sci. Technol. A **6**, 2390, (1988).

[21] R. Cuerno and A. -L. Barabási, Phys. Rev. Lett. **74**, 4746 (1995).

[22] S. Habenicht, K. P. Lieb, J. Koch, and A. D. Wieck, Phys. Rev. B **65**, 115327 (2002).

[23] A. K. Hartmann, R. Kree, U. Geyer, and M. Kölbel, Phys. Rev. B **65**, 193403 (2002).

[24] P. Sigmund, Phys. Rev. **184**, 383 (1969).

[25] M. Siegert and M. Plischke, Phys. Rev. E **50**, 917 (1994).

[26] P. Šmilauer, M. R. Wilby, and D. D. Vvedensky, Phys. Rev. B **47**, 4119 (1993).

[27] F. Frost, A. Schindler, and F. Bigl, Phys. Rev. Lett **85**, 4116 (2000).

[28] M. Feix, A. Hartmann, R. Kree, J. Muñoz-García, and R. Cuerno, in preparation

[29] S. Das Sarma and P. Tamborenea, Phys. Rev. Lett. **66**, 325 (1991)

[30] M.R. Wilby, D.D. Vvedensky, and A. Zangwill, Phys. Rev. B **46**, 12896 (1992); **47**, 16068 (E) (1993)

[31] M.V. Ramana Murty and B.H. Cooper, Phys. Rev. Lett. **83**, 352 (1999)

[32] K. Malarz and A.Z. Maksymowicz, Int. J. Mod. Phys. C **10**, 659 (1999)

[33] S.V. Ghaisas, Phys. Rev. E **63**, 062601 (2001)

[34] P. Punyindu Chatraphorn, Z. Toroczkai, and S. Das Sarma, Phys. Rev. B **64**, 205407 (2001)